Training and Deploying Computer Vision Models for Indoor Localisation

Mika Senghaas
IT University of Copenhagen
jsen@itu.dk

A Thesis presented for the Degree of
Bachelor of Science in Data Science

IT UNIVERSITY OF CPH

IT University of Copenhagen
Computer Science Department

May, 15th 2023

Contents

Abstract

Current indoor localisation technologies require rigorous fine-tuning to the task at hand, high maintenance efforts and don't scale well, making commercial applications rare. In this context, and in the light of the success of deep learning in numerous computer vision tasks, this study proposes to phrase indoor localisation as a classification task in applications which do not require centimetre-level accuracy. Various deep learning architectures, including convolutional, residual, densely connected and self-attention based models, are trained and evaluated on a self-collected indoor video dataset for localisation. The best performing models exhibit capabilities for generalisation and robustness to varying input in a low-resource data setting - giving hope for this approach to become a viable alternative to existing technologies.

1 Introduction

With the introduction of GPS (Global Positioning System), a satellite-based positioning system, localisation in outdoor spaces has become more efficient and accurate than ever before. Gradual commercialisation led to the technology rapidly transforming industries and personal navigation. Today, outdoor localisation is widely considered a *solved problem*.

The same cannot be said for indoor localisation. Because the transmitted radio signals sent out by the satellites in GPS systems are not strong enough to penetrate through walls and struggle with reflections from large buildings, the technology yields inaccurate results at best, and often becomes dysfunctional in indoor spaces *[CITE]*.

Finding alternative solutions to provide an accurate, cheap and robust indoor localisation systems has been a main focus of research in the past decades, and is becoming increasingly important in the light of the ongoing urbanisation of our living spaces and the emergence of autonomous robots and vehicles in our everyday life. Decades of research have led to the development of a variety of different indoor localisation technologies. Hardware-based systems use radio signals, transmitted by beacons, like Bluetooth [4, 6], and Ultra-Wideband (UWB) [2, 3] or Wi-Fi [15, 19, 28], to localise an agent in a known environment. Software-based systems, like Simultaneous Localisation and Mapping (SLAM) [8, 20, 25] algorithms, use sensory information, like cameras or distance-measuring laser sensors, as input to a complex pipeline involving various computer vision algorithms to ultimately localise an agent in an unknown environment, while also building a map of the environment.

While these approaches have proven to produce remarkable results, being capable of localising an agent with centimetre accuracy, they are limited for various reasons: Hardware-based system require an expensive initial setup, continuous maintenance of the signal-transmitting beacons, and are often not feasible in large environments *[CITE]*. SLAM algorithms, on the other hand, require a meticulously handcrafted pipeline of feature detection, feature matching, and pose estimation that has to be fine-tuned by experts for each indoor space, to achieve outstanding results *[CITE]*. All of the above short-comings of existing indoor localisation technologies make commercial applications rare and not unified in their approach.

Previous approaches were designed under the assumption that centimetre-accuracy is categorically required. However, this is not always the case. For some applications, like indoor navigation, it is sufficient to know the position of the agent with a meter or even room-accuracy, instead of centimetre accuracy. One example of such an application is the navigation in large indoor spaces, like airports, train stations, or shopping malls, where the goal is to guide the agent to a specific room or area. In these cases, the constraint of centimetre-accuracy can be relaxed, in favour of a simpler and more versatile solution.

In the past decades, deep learning has proven to be a powerful tool in a wide-variety of tasks and has repeatedly proven remarkable capabilities in the field of computer vision. Amongst common tasks in computer vision are of image and video classification, where the goal is to predict a label from a set of pre-defined labels for a given image or video.

Motivated by the apparent lack of a simple, unified indoor localisation system and the success of deep learning in computer vision, this study investigates the applicability of modern deep learning techniques to the task of indoor localisation when viewing localisation as a classification task. The study presents the rigorous evaluation of several modern deep learning architectures on a challengingly small video dataset for mapping out a novel indoor space.

2 Background

Creating accurate, robust and cheap indoor localisation systems is not a novel task, but has been a focus of research at the intersection of robotics, computer vision and machine learning for decades.

2.1 Hardware-Based Indoor Localisation

The approach conceptually closest to GPS-based outdoor localisation systems are hardware-based indoor localisation systems. Because radio signals transmitted by satellites are incapable of penetrating through walls, various close-proximity radio signals have been proposed to be used for indoor localisation, such as Bluetooth [4, 6], Ultra-Wideband (UWB) [2, 3] or Wi-Fi [15, 19].

No matter the radio signals, three main approaches can be distinguished: (1) Angle of Arrival (AOA), (2) Time of Arrival (TOA) and (3) RSSI-Fingerprinting (RSSI-FP) [19].

In AOA approaches, transmitting beacons, called access points (APs), are measuring the distance and angle between a beacon and an agent. The intersection between the lines of sight (LoS) of at least three APs yields the position of the agent.

TOA approaches (such as GPS) use the received signal strength (RSS) to estimate the distance between an agent and the AP through a propagation model. Given the distance estimates of at least four APs, the agent's position can be determined by an approach called multilateration, which is based on the idea that an agent's position in three-dimensional space can be uniquely determined by the intersection of four spheres with known radius and centres. Clearly, TOA approaches require knowledge about the position of the APs, which makes them less practical in indoor spaces, where the position of the APs is often unknown.

The approach with the most recent research interest is RSSI-FP. It can be divided into two separate phases: In an offline mapping phase, the indoor environment is mapped by repeatedly measuring the received signal strength indicator (RSSI) values of the APs at various reference points (RPs). A vector of RSSI values then uniquely identifies each RP and is stored in a database. In the online localisation phase, the agent's position is then determined by dynamically comparing the agent's RSSI vector against the RSSI vectors of the RPs stored in the database. Ultimately, the agent's position is determined as the position of the RP with the most similar RSSI vector according to some similarity metric. While this approach alleviates the need for the precise positions of the APs, it requires a time-intensive offline mapping phase and is sensitive to changes in the environment.

Many of the proposed technologies assume massive infrastructure deployments and incur high setup and maintenance costs. Wi-Fi based approaches seem most promising, given their ubiquitous availability in modern indoor spaces. However, all hardware-based approaches suffer measurements errors that underlie the triangulation (AOA), multilateration (TOA) or fingerprinting (RSSI-FP) approaches. Such errors are caused by reflections (multipath effect), blockage (shadowing), and signal attenuation (fading) *[CITE]*.

2.2 Simultaneous Location and Mapping (SLAM)

Amongst the most promising approaches are SLAM (Simultaneous Localisation and Mapping) algorithms. SLAM algorithms aim to localise an agent inside an unknown environment, while simultaneously building a consistent map of the environment. There exist a variety of different approaches to SLAM, depending on the type of sensors that are used. For example, Visual SLAM (V-SLAM) algorithms use camera input, and LidarSLAM algorithms use distance-measuring laser sensors.

Most related to this study are monocular V-SLAM algorithms, because they use a single camera to estimate the position of the agent. The very first monocular feature-based V-SLAM algorithms, MonoSLAM, was proposed in 2007 [8]. The research is considered a break-through in V-SLAM algorithms, as it is considered the first algorithm producing accurate results while only using a single camera. Previously, V-SLAM algorithms required multiple cameras or other sensors to overcome the problem of depth estimation using a single camera.

Since then, many adjustments and optimisation have been proposed to the algorithm to make it more robust and accurate. Typically, the adjustments replace or modify one of the components of the pipeline. For example, the ORB-SLAM [25] algorithm uses a bag-of-words approach for feature matching, and the PTAM [20] parallelises the computation for positioning and map creation, which was shown to improve the accuracy of the algorithm. In recent years, modifications are often based on deep learning techniques to improve parts of traditional SLAM pipelines. For example, the DeepVO [33] algorithm uses a convolutional neural network to estimate the camera pose from a sequence of images.

Overall, SLAM algorithms are promising for indoor localisation due to their precision and simultaneous map creation. This makes them state-of-the-art for autonomous robots, which are required to localise themselves in unknown environments. However, SLAM algorithms are computationally expensive and require a lot of memory. This makes them less suitable for mobile devices, which are often resource-constrained. Furthermore, to achieve outstanding results, the SLAM pipeline needs to be fine-tuned to the specific environment and use-case, which can only be done by experts. This makes SLAM algorithms less suitable for general-purpose indoor localisation.

2.3 Deep Learning in Computer Vision

Computer vision is one of the major subfields of artificial intelligence and is concerned with the automatic extraction of information from images. The extraction of information from images is not straight-forward, because images are high-dimensional and unstructured. This makes it a challenging environment for hand-crafted algorithms, which are often based on heuristics and assumptions about the data. For this reason, deep learning techniques have been applied successfully to many computer vision tasks.

The most prevalent architectural paradigm in computer vision is the convolutional neural network (CNN). CNNs are a type of neural network, which are inspired by the visual cortex, which is responsible for processing visual information. Like the visual cortex, CNNs are organised hierarchically and consist of a stack of convolutional layers. In each layer, a convolutional filter is applied to the input, which is then passed to the next layer. For image data, the convolutional filter is a three-dimensional matrix of weights that is moving alongside two dimensions (width and height) of the input, and is therefore referred to as 2d-Convolution. For video data, the convolutional filter is a four-dimensional matrix of weights that is moving alongside three dimensions (width, height, and time) of the input, and is therefore referred to as 3d-Convolution. The output of a convolutional layer for each region is computed as the dot product of the filter and the input region. A convolutional layer is typically parametrised by the number, size and stride of filters.

While the theory behind CNNs was already established in the 1980s [22], practical applications were limited by the lack of computational power and large datasets. The offset of the deep learning wave in computer vision was the success of the AlexNet [21] architecture in the 2012 ImageNet Large Scale Visual Recognition Challenge [9], which crushed the competition by increasing the Top-5 Accuracy from 73.8% to 84.7%.

In the following years, CNN-based architectures with increasing depth and width, and architectural improvements, such as weight initialisation, batch normalisation, residual connections [26, 27, 14, 7] were proposed and pushed the state-of-the-art further. The introduction of ResNet in 2015 is considered a cornerstone in convolutional neural networks architectures, as it allowed for the training of much deeper networks without the problem of vanishing gradients. With the success of Transformer-based architectures for language modelling in natural language processing [32], the computer vision community was quick to adapt the architecture to computer vision tasks. The first successful application of the Transformer architecture to computer vision was the Vision Transformer (ViT) [11], which achieved state-of-the-art on many image classification benchmarks [9].

Beyond image classification, the task of video classification has recently gained traction with the introduction of large-scale video datasets, such as Kinetics [18], more computational resources and an increasing need to understand video data in a multi-media world. Continuously predicting on a stream of frames is related to image classification, but adds complexity to the task through the temporal dimension and increase in data size. Video classification can be solved by combining CNNs with recurrent neural networks (RNNs) or by using 3D convolutions. The first approach by Donahue et. al proposes long-term recurrent convolutional networks (LRCNs), which use a CNN to extract features from each frame, which are then fed into a LSTM [10] to produce a sequence of predictions. Current state-of-the-art approaches leverage the 3D convolution operation to capture the spatio-temporal nature of video data [30, 5]. Yet another approach, called SlowFast [13] uses two separate CNN networks to capture spatial and temporal information separately, which are then combined in the final layers of the network.

3 Methodology

Within this study, we will investigate the use of deep learning techniques for indoor localisation when framed as a classification task. We differentiate between two types of problem settings throughout the entire report:

1. **Single-frame classification**: Given a continuous stream of frames, a video, the task is to classify each frame individually.
2. **Video classification**: Given a continuous stream of frames, a video, the task is to classify fixed-sized clips of the video.

The following sections describe the data collection, pre-processing, annotation, models, training and evaluation procedure for all experiments conducted within this study.

3.1 Raw Data

Framing the problem of indoor localisation as a classification task requires a labelled data set, which consists of sequentially-arranged pairs of inputs and outputs, that map visual information to location labels. Both problem settings are based on the same raw data, which is described in the following.

The raw data was collected from a single camera of a mobile device at a frame rate of 30 FPS in high resolution (2426×1125). The mobile device was hand-held by a human agent while walking around the main building of the Southern Campus of the Copenhagen University (Danish: Københavns Universitet, KU) in Copenhagen S, Denmark. The building is a large multi-storey building with a total of six floors, and is used for teaching and research purposes. The location was deemed compatible with this study, as it showcases distinctive learnable indoor features (e.g. coloured walls, unique structures, etc.), but also challenges the model, for example, due to the similarity of the floor plan across floors. For the scope of this project, the data collection was limited to the first two floors. This process yielded a set of videos $V = \{v_1, ..., v_n\}$, where each video v_i is a sequence of k frames $f_0, ..., f_k$. Each frame f_i is a RGB image, represented as a three-dimensional tensor of shape $3 \times h \times w$, where h and w are the height and width of the image, respectively.

The raw data also consists of a set of location labels $L = \{l_1, ..., l_n\}$, where each location label l_i is a scalar value, which identifies the location of the agent at the time of the frame. For the scope of this project $|L| = 20$ different location labels were considered. The location labels are identified with a descriptive name and are shown in Figure 1 alongside the coloured regions, which represent are represented by the location labels. Whenever possible, the location labels were designed in close correspondence to the building's official floor plan.

Annotation was performed manually by a single human agent. Because changes in the location labels only occur at the transition of rooms, the annotation process was simplified by annotating the starting and ending time stamps of a location label, which were later pre-processed to frame-by-frame annotations.

A total of $n = 53$ videos of varying length were recorded, with an average duration of ~ 57s, amounting to a total number of ~ 50 minutes of footage, or an equivalent of $\sim 90K$ frames. Out of the total 53 videos that were recorded, 37 were used for training and 16 were used for testing. Importantly, the videos in the training split were recorded in a single session, while the videos in the test split were recorded on four separated days, in a span of two to four weeks after the training data had been recorded. This ensured that the trained model could be tested against unseen data, to more accurately assess its generalisation capabilities.

3.2 Processed Data

A video classification models expects a single clip c_i as input, which is a sequence of s_v frames sampled from a video v_i at a sampling rate r_v. The number of frames per clip s_v and the sampling rate r_v are tied to the model architecture and are therefore fixed for each video classification model (Details in Section 3.3). Clips are extracted in uniformly spaced intervals, which means that the number of clips k_v that can be extracted from a video v_i with k frames is $\lfloor k/(r_v \cdot s_v) \rfloor$. The trailing frames that cannot be extracted as a clip are discarded. Each of the k_v clips contains s_v frames, leading to a total of $\lfloor k/(r_v \cdot s_v) \rfloor \cdot s_v$ frames for a single video.

Single-frame classification models expect a single frame f_i from a video v_i as input. Technically, all frames in a video v_i could be used as input, but because of the strong local correlation between adjacent frames, it was hypothesised that models would overfit to the training data. For this reason, and in an attempt to make the training procedure more similar to the video classification models,

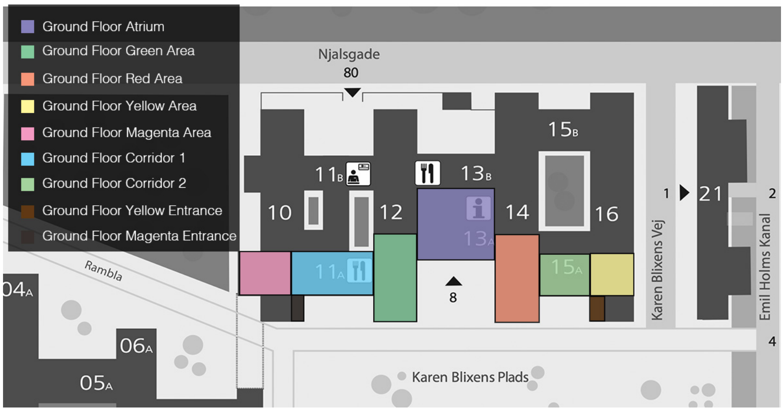

(a) Ground Floor

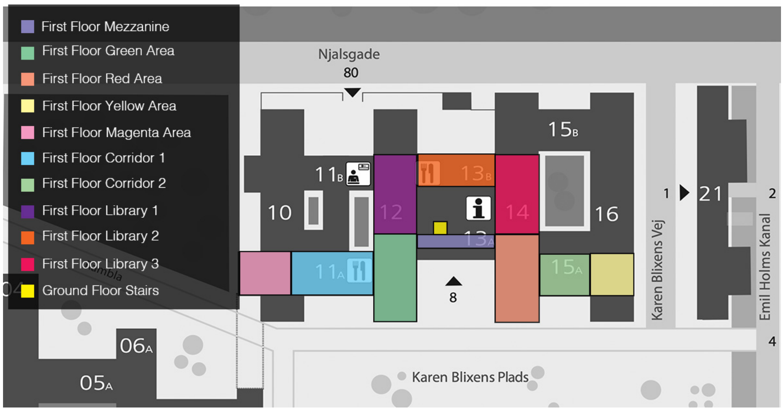

(b) First Floor

Figure 1: **Floor Plan of the Southern Campus of the Copenhagen with Location Labels.** The coloured regions represent the $|L| = 20$ location labels as distributed over the two floors in the indoor space. It is apparent that a) the floor plan is similar across floors and b) that locations significantly differ in size.

a frame f_i is sampled from a video v_i at a sampling rate r_f. Here, r_f is not tied to the model architecture and can be chosen freely. For all experiments r_f was chosen to be 30 for all single-frame classification, meaning only every 30th frame was sampled from a video. The number of frames k_f that can be extracted from a video v_i with k frames is $\lfloor k/r_f \rfloor$. It becomes clear that the frames considered per video k_f is similar to the number of frames considered as part of clips if the two sampling rates r_v and r_f are equal, as

$$\left\lfloor \frac{k}{r_v \cdot s_v} \right\rfloor \cdot s_v \approx \left\lfloor \frac{k}{r_f} \right\rfloor, \quad \text{if} \quad r_v = r_f$$

The extraction of clips and frames for video and single-frame classification models, respectively, is illustrated in Figure 2. It shows that despite the same raw data source, the frames considered in the two datasets are not the same. This is because the frames in the video dataset are potentially sampled at a different rate than the frames in the single-frame dataset and because adjacent clips reset the sampling rate. However, due to the large number of total frames and strong local correlation between adjacent frames, the two datasets are sufficiently similar to allow for comparison between the two model types.

Figure 2: **Data Extraction.** A raw video with $k = 10$ frames is processed into $k_f = 5$ frames for the single-frame dataset and $k_v = 2$ clips for the video dataset. Samples for each dataset type are indicated by a surrounding box. Frames are sampled at a rate of $r_f = 2$ for the single-frame dataset and $r_v = 3$ for the video dataset. A clip contains $s_v = 2$ frames. Frames are colour-coded in correspondence to the dataset they belong to (single-frame dataset in purple and video dataset in blue), if they are sampled to the respective dataset. Discarded frames are coloured in grey (light-grey for within video frames, dark-grey for trailing frames).

Both the image and video classification models expect a single sample x_i, whether it be a frame or a clip, to be standardised and of a certain size. Standardisation is performed on a per-channel basis after normalising the input to the range $[0, 1]$. Then, a sample x_i is standardised as,

$$x'_{ic} = \frac{x_{ic} - \mu_c}{\sigma_c} \quad \text{for} \quad c \in \{1, 2, 3\}$$

, where x_{ic} represents the channel c of the sample x_i and x'_{ic} is the standardised channel c of the sample x_i. μ_c and σ_c are taken from the ImageNet dataset [9] for image classification models and from the Kinetics dataset [18] for video classification.

The height and width of each input frame is tied to the model architecture and is therefore fixed for each model. Input sizes are typically square and range from 182×182 to 224×224 for all models (Detail in Section 3.3). Resizing is performed in a non aspect-preserving manner to compress as much of the original viewport as possible into the resized frame. However, this also means that the trained models are likely to only perform well on frames with a similar raw aspect ratio as the training data (at least should be in portrait model).

After all processing steps, the single-frame dataset contains n_f samples and the video dataset contains n_v samples. The number of samples n_f and n_v is dependent on the number of videos n and the number of frames k in each video. The final single-frame dataset can be written as $D_F = \{(f_1, y_1), ..., (f_{n_f}, y_{n_f})\}$, and the final video dataset as $D_V = \{(c_1, y_1), ..., (c_{n_v}, y_{n_v})\}$.

3.3 Models

A deep learning model is supposed to learn a function $f : X \to Y$, where X represents the input space and Y the output space. In both single-frame and video classification, the output space is the discrete set of location labels, $Y = L = \{l_1, \ldots, l_n\}$. The input space X is different for the two model types, as described in Section 3.2.

A total of 10 different models are trained and evaluated in this work. The models are split into two categories: single-frame classification models and video classification models. The single-frame classification models are trained on the single-frame dataset D_F and the video classification models on the video dataset D_V. A comprehensive overview of the models is given in Table 1. The models are described in detail in the following.

	Model	**Release** (Y)	**Rate** (r_f/r_v)	**F/C** (s_v)	**Size** (h, w)	**Params** (M)	**FLOPs** (G)	**Acc@1** (%)
Single-Frame	AlexNet [21]	2012	30	-	224	61.1	0.71	56.52
	GoogLeNet [27]	2014	30	-	256	6.6	1.5	69.78
	ResNet18 [14]	2015	30	-	224	11.7	1.82	82.52
	ResNet50 [14]	2015	30	-	224	25.6	4.09	80.86
	DenseNet 121 [17]	2016	30	-	224	7.0	2.88	74.43
	MobileNet V3 [16]	2019	30	-	224	3.5	0.32	71.88
	ViT-B-16 [11]	2020	30	-	224	86.7	17.56	81.07
	EfficientNet V2 S [29]	2021	30	-	224	21.5	8.37	84.23
	ConvNext Tiny [23]	2022	30	-	224	28.2	4.46	82.52
Video	R(2+1)D [31]	2018	4	16	182	28.11	76.45	76.01
	X3D S [12]	2020	6	13	3.5	182	2.96	73.33

Table 1: **Model Overview.** The table shows all models that were evaluated in this work. The models are split into two categories: single-frame models and video models. For each model, the table reports the release year (Release), the frame rate (Rate) of the training data, the number of frames per clip (F/C; *only applicable to video classifiers*), the spatial resolution (Size) of the input images, the number of parameters in millions (Params), the number of floating point operations in billions (FLOPs) and the Top-1 accuracy (Acc1) on ImageNet [9] for single-frame classification models and the top-1 accuracy on the Kinetics [18] dataset for video classification models. The table is sorted by release date within each group.

Alexnet is a convolutional neural network that was introduced by Krizhevsky et al. [21] in 2012. It was the first deep neural network to win the ImageNet Large Scale Visual Recognition Challenge [9] and is considered to be one of the first successful application of deep learning to image classification. Architecturally, it uses the standard building blocks of convolutional nets. It consists of 5 convolutional layers (with filter sizes of 11×11, 5×5 and 3×3) with occasional max-pooling layers in between, followed by 3 fully connected layers. The network uses the ReLU activation function and dropout for regularization.

GoogLeNet is a convolutional neural network that was introduced by Szegedy et al. [27] in 2014. At its core, it is based on Inception modules, which allow the network to choose between multiple convolutional filter sizes in each block. Each inception module consists of 4 parallel convolutional layers, whose outputs are concatenated along the channel dimension. This advancement allowed the Google Team to significantly reduce the number of parameters in the network and win the ImageNet Large Scale Visual Recognition Challenge [9] in 2014.

ResNet was introduced by He et al. [14] in 2015. The main contribution of ResNet is the residual block, which allows the network to learn residual functions with respect to the layer inputs. This allows the network to be trained much deeper than previous architectures. The original ResNet paper introduced several architectures with different depths. In this work, we use ResNet18 and ResNet50, which are among the smallest architectures in the family.

Densenet was introduced by Huang et al. [17] in 2016. The main contribution of Densenet is the dense block, which allows the network to learn feature maps from all preceding layers. This allows the network to be trained much deeper than previous architectures. The original Densenet paper introduced several architectures with different depths. In this work, we use Densenet121, which is among the smallest architectures in the family.

MobileNet V3 was introduced by Howard et al. [16] in 2019. The main contribution of MobileNet V3 is the efficient inverted bottleneck block.

ViT was introduced by Dosovitskiy et al. [11] in 2020. It is the first attempt to apply the Transformer architecture proposed by Vaswani et. al [32] to computer vision task. The main contribution of ViT is the patch embedding mechanism, which allows to transform a two-dimensional image into a one-dimensional sequence of tokens that, alongside a positional encoding, can be processed by the Transformer architecture. The original ViT paper introduced several architectures with different depths. In this work, we use ViT-B-16, which uses a patch dimension of 16×16.

EfficientNet V2 was introduced by Tan et al. [29] in 2021.The main contribution of EfficientNet V2 is the efficient inverted bottleneck block, that also underlies MobileNet V3 [16].

ConvNext is the most recent model in this work. It was introduced by Wang et al. [23] in 2021, producing state-of-the-art results.

R(2+1)D was introduced by Tran et al. [31] in 2018. It is the first attempt to apply the ResNet architecture [14] to video classification tasks. The main contribution of R(2+1)D is the spatiotemporal convolutional block, which allows the network to learn spatiotemporal features. The original R(2+1)D paper introduced several architectures with different depths. In this work, we use R(2+1)D-18.

X3D was introduced by Feichtenhofer et al. [12] in 2020. *TBD*.

3.4 Training

All models were implemented using the `PyTorch` framework [1] and the training was performed remotely on the high performance cluster (HPC) of the IT University of Copenhagen. A single node with GPU acceleration was used for training. For more details on the hardware specifications see the Appendix (Section 7).

During training, all models were evaluated using the standard multi-class loss function cross-entropy loss (Equation 1), which is defined as,

$$\mathcal{L}(\hat{\mathbf{y}}, \mathbf{y}) = -\sum_{i=1}^{L} \mathbf{y}_i \log(\hat{\mathbf{y}}_i) \quad . \tag{1}$$

Here, $\hat{\mathbf{y}}$ is the predicted probability distribution over the L location labels and $\mathbf{y}$ is the one-hot encoded ground truth location label.

All models were trained using the AdamW [24] optimiser with default parameters, except for the learning rate, which was set to a constant of $1e^{-4}$. The batch size was set to 32 for all single-frame classifiers and 4 for all video classifiers due to memory limitations. Unless otherwise specified, all single-frame and video classifiers were trained with the same set of training hyper-parameters, which are specified in Table 2.

Classifier	Batch Size	Epochs	Optimiser	Learning Rate Scheduler
Single-Frame	32	10	AdamW ($\gamma = 1e^{-4}$)	Step-LR ($\gamma = 1e^{-1}, s = 5$)
Video	8	10	AdamW ($\gamma = 1e^{-4}$)	Step-LR ($\gamma = 1e^{-1}, s = 5$)

Table 2: Default Hyperparameters for Single-frame and Video classifiers

3.5 Evaluation

To assess all models in terms of their performance and efficiency on the task of location classification, a series of different performance and efficiency metrics are computed. All metrics are computed on the test set, which was separated from the original dataset before training, as described in Section 3.1.

The accuracy of the models is evaluated using the standard multi-class top-1 and top-3 accuracy metric. It is the ratio of samples, for which the correct label is among the top-1 or top-3 predictions, respectively. As some location labels are naturally underrepresented in the dataset due to the natural variation in size of the different locations, the macro F1-score is used to compute a more fine-grained metric that gives more weight to resource-constrained locations. The macro F1-score is the average of the class-specific F1-scores, which are defined as the harmonic mean of precision P_i and recall R_i. All performance metrics where computed using the `TorchEval` library *[CITE]*.

To assess the efficiency of the models a series of benchmarks were performed on the HPC. The benchmarks were performed using the `PyTorch Benchmark` library. The library allows to track various metrics during unbatched and batched inference. Results are aggregated over 5 passes and the mean and standard deviation are reported. Out of all computed metrics, the mean inference time per sample (latency) and mean number of samples per second (throughput) were further considered.

Due to different nature of the underlying datasets D_f and D_v, the performance and efficiency metrics are not directly transferable. For example, the top-1 accuracy of the single-frame classifiers is the number of correctly predicted frames, whereas the top-1 accuracy of the video classifiers is the number of correctly predicted videos. While this limits the comparability of the metrics, it is still possible to draw conclusion between the different model types due to the relatively large number of samples and the natural resemblance of frames and clips.

To analyse the model behaviour in more detail, the models were also evaluated qualitatively by manually inspecting the confusion matrix and a subset of the misclassified samples for the best-performing single-frame and video classification model.

4 Results

We show that computer vision models, when carefully designed and trained, are generally capable of solving the task of indoor localisation when phrased as a coarse-grained classification problem. The results of the evaluation are presented in Table 3.

	Model	Acc@1 (%)	Acc@3 (%)	Ma.-F1 (%)	FLOPs (G)	Latency (ms/Pred)	Throughput (Preds/s)
Single Frame	AlexNet	56.67	81.36	50.79	0.71	14.1	70.91
	Google LeNet	63.40	84.74	56.80	1.97	47.2	21.17
	DenseNet121	67.79	83.04	63.05	2.88	71.9	13.89
	ResNet18	70.65	89.73	64.84	1.82	27.1	37.22
	ResNet 50	55.76	77.65	50.05	4.12	60.9	16.41
	MobileNet V3 Small	28.68	51.34	19.21	0.06	**11.9**	**83.82**
	ViT B-16	53.20	77.57	47.54	17.59	166.0	6.03
	EfficientNet V2 Small	50.51	81.73	41.71	2.88	77.6	12.91
Video	R(2+1)D	**78.33**	**91.67**	**75.27**	**93.72**	825.1	1.22
	X3D	68.89	81.11	54.09	2.85	229.0	4.37

Table 3: **Results.** The table the performance and efficiency metrics for all trained models. The models are grouped by their type (single-frame or video). The performance metrics are the top-1 accuracy (Acc@1), top-3 accuracy (Acc@3) and Macro F1-Score (Ma.-F1). The efficiency metrics are the number of floating point operations (FLOPs) per inference, the mean inference time in milliseconds per prediction (Latency) and the mean number of predictions per second (Throughput). The best performing model in each category is highlighted in bold. The metrics are computed on the test set of the respective dataset.

4.1 Detailed Analysis of Single-Frame Classifiers

Surprisingly, even simple single-frame classification models are capable of providing a reasonable solution to the task of indoor localisation. Despite the lack of information about the temporal context of the frames, the best-performing single-frame classifier (ResNet18) achieves a top-1 accuracy of 70.65% and a top-3 accuracy of 89.73%. This is a significant result as it shows that processing single frames of the video is sufficient to solve the task of indoor localisation. This is especially important in the context of mobile devices, and applications where real-time inference is required.

Out of the single-frame classifiers, three classifiers can produce real-time predictions on a mobile device, as they have a higher throughput rate than video frame rate. The most efficient model is MobileNet V3 with a throughput of 83.82 predictions per second. AlexNet and ResNet18 are also capable of real-time inference with throughputs of 70.91 and 37.22 predictions per second, respectively. All other models are not capable of real-time inference on a mobile device, but are sufficiently quick to provide near real-time predictions.

Evidence in computer vision research suggests that more complex models typically are able to achieve better performance. This is not entirely the case for this study. The smallest model, MobileNet V3, is a clear outlier in terms of performance, only achieving a top-1 accuracy of 28.68%. It is hypothesised that the model is not complex enough to handle the challenging 20-class classification task. As models are getting more complex, the performance increases up until the complexity of ResNet18 (11.2M parameters). All models with a higher number of parameters than ResNet18 perform worse. Interestingly, the most complex model in terms of the total number of parameters, ViT-B-16 (85.8M), which achieves state-of-the-art results on common image classification benchmarks, is not the best-performing model in this study. This is likely due to the small size of the dataset in combination with relatively few training epochs.

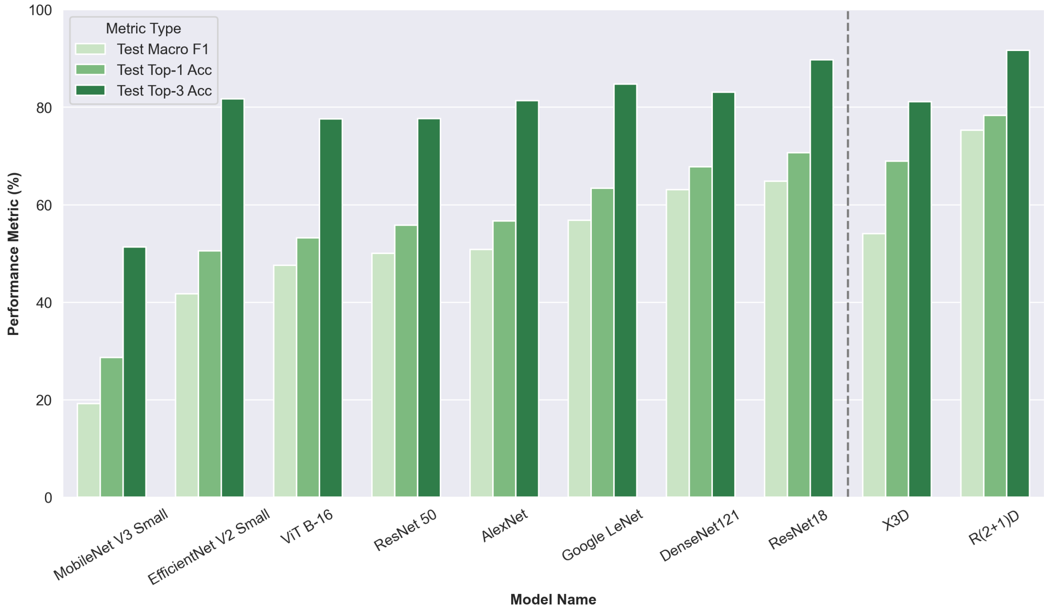

Figure 3: **Performance Metrics.** The Figure shows the performance metrics, Macro F1, Top-1 Accuracy and Top-3 Accuracy, for all trained models on the test split. A grey, dotted line separates the single-frame classifiers (left) from the video classifiers (right). Within their group, models are sorted from left to right by their Top-1 Accuracy.

4.2 Detailed Analysis of Video Classifiers

As the nature of the task is inherently temporal, it is not surprising that video classifiers outperform single-frame classifiers (Figure 3). The best performing video classifier is R(2+1)D with a top-1 accuracy of 78.33% and a top-3 accuracy of 91.67%. This is a significant improvement over the best performing single-frame classifier, ResNet18. The video classifiers are more robust to noise in the input data, as they are able to leverage the temporal context of the video. For example, the model is capable of predicting a clip correctly despite a few frames being occluded by a person walking through the scene or other sources of noise. This capability has proven especially useful in the context of indoor localisation, as high variation in the environment and therefore high noise in the input data is common.

Video classifiers generally require more compute and memory resources during inference, as they have to keep a history of the previous frames in memory. This is reflected in the efficiency metrics. R2+1D has a throughput of only 1.22 predictions per second. This means that it can only provide predictions for the location every second. This makes the model slower in responding to sudden changes in the environment.

4.3 Performance Efficiency Trade-Off

The pre-dominant tendency in deep learning is that with sufficient data sizes and compute resources, more complex models outperform simpler ones. However, there is a trade-off between model complexity and efficiency, when inference time is critical like when deployed on a mobile device.

Figure 4 shows the Top-1 Test Accuracy of all models against latency (left) and throughput (right).

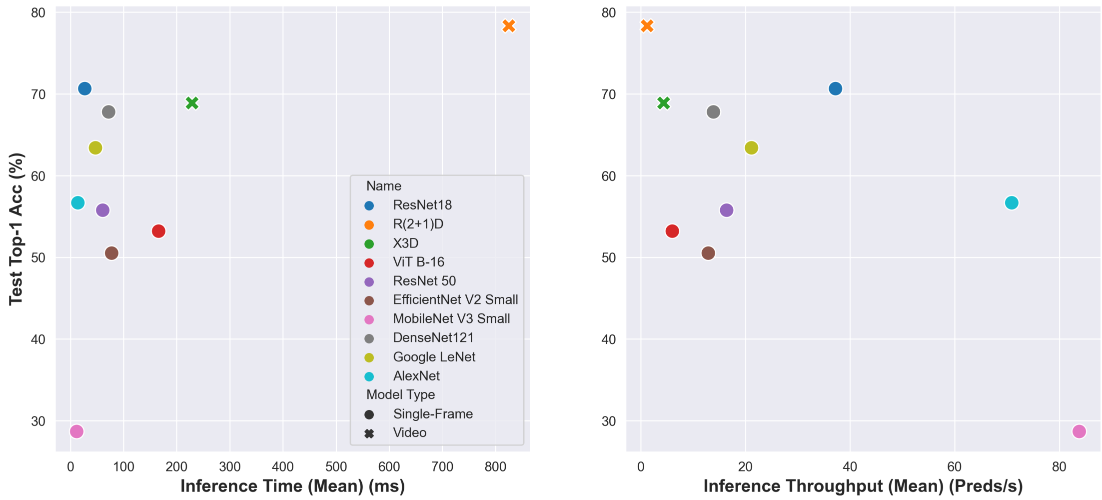

Figure 4: **Performance-Efficiency Trade-Off.** The Figure visualises the performance-efficiency trade-off for all models by plotting the relationship between the Top-1 Accuracy against the latency (inference time in milliseconds per prediction) and throughput (predictions per second). Each model is given unique colour, and the marker type indicates whether the model is a single-frame classifier (circle) or a video classifier (cross).

Latency and throughput are meaningful metrics to assess model's efficiency, as they are a direct proxy for the real-time inference speed when deployed on low-resource device. While the benchmarks were computed on a desktop CPU, they give a good indication of the relative performance of the models and allow to extrapolate the insights to performance on a mobile device. It is to be noted that latency and throughput are inversely proportional to each other: Less inference time per sample (low latency) leads to a higher number of inferences per second (high throughput). However, as inference times vary greatly between models, the two metrics are plotted separately, as they highlight different tails of the distribution. Specifically, the latency plot accentuates high latency models, while the throughput plot highlights low latency models.

In Figure 4a, R(2+1)D is a clear outlier. The model has the highest latency, but also the best overall performance. The increase in complexity over X3D seems to be justified, as the model achieves a 9.4% increase in Top-1 Accuracy, while only increasing the latency by 0.6 seconds. A similar trend cannot be observed for the single-frame classifiers. As latency times are close to each, their trend is easier to study in Figure 4b. Here, a quadratic relationship between throughput and accuracy can be observed for the single-frame classifiers. High-complexity, but low-throughput models, like ViT-B-16, EfficientNet V2 S and ResNet18 are outperformed by lower-complexity models. Similarly, low-complexity, but high-throughput models, like MobileNet V3 and AlexNet, show similarly low performance. The sweet spot in terms of throughput and accuracy is ResNet18, which achieves a throughput of 37.22 predictions per second and a top-1 accuracy of 72.92% This phenomenon is best explained by the fact that low-complexity models are not able to capture the complexity of the task, while high-complexity models are not able to learn from the small dataset. The video classification models defy this trend, as they are all low-throughput, but high-performing.

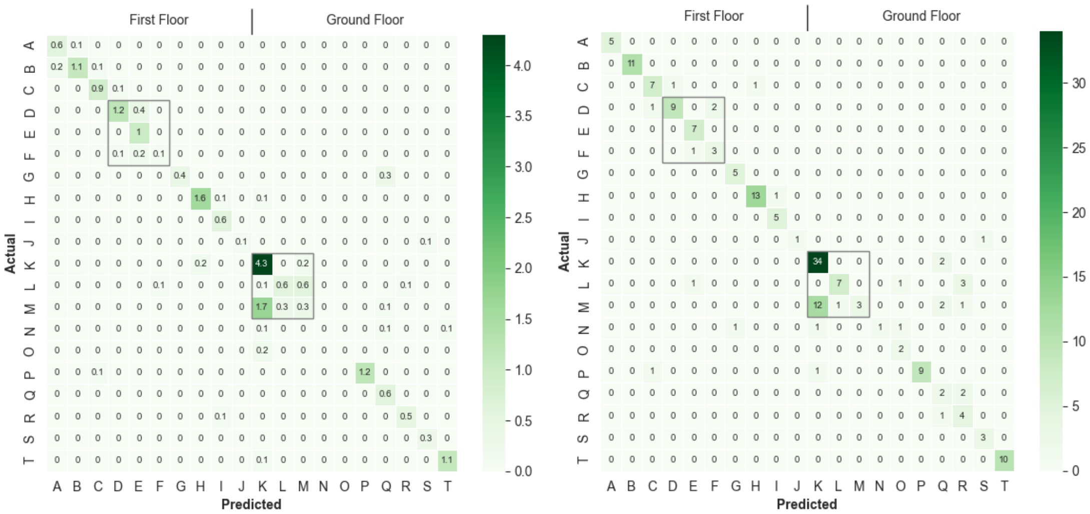

(a) ResNet18

(b) R(2+1)D

Figure 5: **Confusion Matrices.** The Figure shows the confusion matrix for (a) ResNet18 (best performing single-frame classifier) and (b) R(2+1)D (best performing video classifier). The confusion matrix of ResNet18 is normalised to show 1K samples per class for visual purposes. For both matrices, the entry at row i and column j shows the number of samples that belong to class i but were predicted to be class j. Gray rectangles indicate challenging classes, that are often confused.

4.4 Analysing Prediction Patterns: Confusion Matrices

To better understand the strengths and weaknesses of deep learning models in tackling the task of indoor classification, the two best performing models, ResNet18 and R(2+1)D, are analysed in more detail. Specifically, the confusion matrices of the two models are analysed to identify common failure modes of the models.

Figure 5 shows the confusion matrices for (a) ResNet18 and (b) R(2+1)D. It becomes clear that both models struggle with the same misclassification scenarios. The most common misclassification is between the two corridors on the ground floor (*Ground Floor Corridor 1* and *Ground Floor Corridor 2*) and the Atrium (bottom-right grey rectangle). ResNet18 both confuses the two corridors and has a tendency for predicting the majority class (Atrium) instead of Corridor 2. R(2+1)D rarely confuses the corridor, but has an even stronger tendency for predicting Corridor 2 as Atrium. These failure cases are explained by the fact that the two corridors and the Atrium are visually very similar. Furthermore, they are directly adjacent to each other, which likely leads to some naturally occurring failure cases at the border of the areas. Here, the model might predict the new class earlier or later than the ground truth label changes.

Another region with similar behaviour are the three libraries on the first floor (*First Floor Library*, *First Floor Library 2*, *First Floor Library 3*). Especially ResNet18 struggles to distinguish between the three classes, which is understandable given the fact that the dominating visual feature of the three classes are rows of bookshelves. R(2+1)D shows a similar, but less pronounced behaviour. One explanation might be that while the shared visual feature of bookshelves, the arrangement of the bookshelves is different in the three libraries, which can be learned by R(2+1)D due to its temporal modelling capabilities.

4.5 Analysing Failing Scenarios: Mispredicted Samples

Figure 6 shows three exemplary mispredicted samples for (a) ResNet18 and (b) R(2+1)D. The respective legend shows the top 3 predicted classes for each sample in order of confidence and the ground truth label.

For ResNet18, the first sample shows a misclassification between the two corridors on the ground floor, which is the most common misclassification for ResNet18 as seen from the confusion matrix (Figure 5a). It can be seen, that the model is unsure about the prediction (64% confidence in Corridor 2 and 34% confidence in Corridor 1). The second and third sample show another common misclassification mode. Here the model confuses the the yellow and green area on the ground and first floor, respectively.

For R(2+1)D, the first sample shows a transition misprediction. The frame is directly at the border between the Magenta Area and Corridor 2 on the ground floor and predicts the Magenta Area, while the ground truth label is Corridor 2. The second sample shows a truly sample from a challenging video from the test split, because the video shows an area that was freshly painted in blue in Corridor 2. As the training split does not contain any videos from this area, the model has never seen this area in blue and thus predicts a wrong area, in this case the majority class Atrium. The third sample shows another misprediction of similar classes. The clip starts at the very end of the entrance with the camera facing to the outside. The model predicts the yellow entrance, when the ground truth label is the magenta entrance.

4.6 Understanding Model Behaviour: Manual Inspection

Finally, the continuous predictions of the two best performing model, ResNet18 and R(2+1)D, are manually inspected on all videos in the test split. The following qualitative observations were made:

1. **Noise Invariance.** Both models show a high robustness to temporal changes in the environment, such as changing lighting conditions, different people in the scene or occlusions. This is especially true for R(2+1)D, which is likely due to the temporal modelling capabilities of the model. However, drastic changes in the environment, such as the repainting of an entire region, lead to consistent mispredictions of the affected area. This is a general drawback of localisation systems that solely rely on the modality of vision

2. **Prediction Robustness.** A noticeable difference in terms of the sample-to-sample variance could be observed. ResNet18 was found more prone to "jittering" predictions, meaning that within a single second, it would predict different classes. Such behaviour was almost entirely absent in R(2+1)D, due to the lower throughput rate and its temporal modelling capabilities.

3. **Low-Resource Classes.** Both models struggle with underrepresented clases and features, like unusual routes or angles. The higher the deviance from the training data, the less certain the models are about their predictions, which often leads to mispredictions. Given this, performance gains are to be expected for large-scale, exhaustive training data collection. In contrast, classes that show distinctive features, such as the Atrium or First Floor Mezzanine, are predicted more reliably.

4. **Training Data Bias.** A bias toward the training data is present in both models. If features that are not representative of a class, but are overrepresented in the training data of that class, there is a chance for the model to learn these features as being indicative of a class. This was the case for the libraries: Most video clips that were taken while walking through bookshelves were filmed in library 2, while the other libraries were filmed in a more open space. This led to model associating in-between bookshelves clips to library 2, even though they are also present

(a) ResNet18

(b) R(2+1)D

Figure 6: **Mispredicted Samples.** The Figure shows the mispredicted samples for (a) ResNet18 and (b) R(2+1)D. The respective legend shows the top 3 predicted classes for each sample in order of confidence and the ground truth label. For the clips from the video classifier, the first frame of the clip is shown.

in the other libraries. When used in practice, data collection has to be carefully designed to avoid such biases.

4.7 Deployment on Mobile Devices

As a proof of concept, the best single-frame classifier, ResNet18, was deployed on a mobile device. The trained model was quantised to 8-bit float precision and converted to `TorchScript` format to be run more efficiently on mobile devices. Deployment was done using the `PlayTorch` framework *[CITE]*, which is a port of the `PyTorch` Mobile SDK for native iOS and Android to Javascript. The deployed model can be tested by downloading the PlayTorch app from the App Store or Google Play Store and scanning the QR code on the right. This will open the application, download the model and run it locally on the device.

5 Limitations & Future Work

This study has shown the potential of using a pure deep learning pipeline for tackling the problem of indoor localisation. However, there are still many open questions that need to be addressed in future work for systems similar to the approach suggested here to be widely useful in real-world applications.

The main drawback of the proposed approach is the coarse location labels. State-of-the-art indoor localisation systems are able to localise users to centimetre accuracy. Therefore, future work should focus making improvements on the entire pipeline that allow for higher precision in the location labels.

Furthermore, this study assumes a small data set of only 40 minutes of video footage for training. While the experiment setup allowed to draw conclusion about the data efficiency of the models and the general feasibility of the data collection and annotation process, it is an open question how similar systems scale to even larger indoor spaces with more training data available.

Additionally, it has to be noted that the test split was collected over a duration of four different days in close succession. Therefore, the test split might not be representative of the true variation of visual inputs from a indoor location over the course of a year. For example, the location might change more significantly than represented in the test split over seasons. In that case, the reported test metrics are likely to be over-optimistic. To gain confidence in favour or against this hypothesis, monitoring the performance of the trained models on test data collected over a longer period of time would be necessary.

Finally, the detailed analysis of the mispredicted samples has shown that most errors, because the models that show a lot of similar features, such as different libraries, or rooms that are architecturally similar across floors. Future work should specifically improve on finding solutions to these issues. Possible starting points might be to use the fact that sudden jumps in the building are impossible, so highly confident predictions from the past can be used as a strong indicator for the next room if some knowledge about the relative position of the rooms is available.

6 Conclusion

The study has shown promising results for the feasibility of a pure deep learning pipeline for indoor localisation.

Surprisingly, the single-frame classifier ResNet18 was able to achieve a test accuracy of 70%. This is a promising result, given that the model was trained on less than 40 minutes of training video footage in a 20 room indoor location. We found that video classification models are able to improve the overall performance of the system noticeably. However, the performance gains come at the cost of a higher computational complexity, which only allows for near real-time inference.

Depending on the application, the trade-off between performance and computational complexity can lead to one or the other architecture being preferred.

All models struggle with low-resource classes, visually similar classes and biases in the training data. All of these issues are grounded in the nature of the data set and the problem itself. Future work should focus on improving the data collection process by, for example, scaling it to larger indoor locations, be mindful of biases in the training data and investigate augmentation techniques to improve the robustness of the models.

References

[1] Pytorch. https://pytorch.org.

[2] N. Alsindi, B. Alavi, and K. Pahlavan. Measurement and modeling of ultrawideband toa-based ranging in indoor multipath environments. *Vehicular Technology, IEEE Transactions on*, 58:1046 – 1058, 04 2009.

[3] N. Alsindi and K. Pahlavan. Cooperative localization bounds for indoor ultra-wideband wireless sensor networks. *EURASIP Journal on Advances in Signal Processing*, 2008, 04 2008.

[4] U. Bandara, M. Hasegawa, M. Inoue, H. Morikawa, and T. Aoyama. Design and implementation of a bluetooth signal strength based location sensing system. In *Proceedings. 2004 IEEE Radio and Wireless Conference (IEEE Cat. No.04TH8746)*, pages 319–322, 2004.

[5] J. Carreira and A. Zisserman. Quo vadis, action recognition? A new model and the kinetics dataset. *CoRR*, abs/1705.07750, 2017.

[6] S. S. Chawathe. Beacon placement for indoor localization using bluetooth. In *2008 11th International IEEE Conference on Intelligent Transportation Systems*, pages 980–985, 2008.

[7] F. Chollet. Xception: Deep learning with depthwise separable convolutions. *CoRR*, abs/1610.02357, 2016.

[8] A. J. Davison, I. D. Reid, N. D. Molton, and O. Stasse. Monoslam: Real-time single camera slam. *IEEE Transactions on Pattern Analysis and Machine Intelligence*, 29(6):1052–1067, 2007.

[9] J. Deng, W. Dong, R. Socher, L.-J. Li, K. Li, and L. Fei-Fei. Imagenet: A large-scale hierarchical image database. In *2009 IEEE conference on computer vision and pattern recognition*, pages 248–255. Ieee, 2009.

[10] J. Donahue, L. A. Hendricks, S. Guadarrama, M. Rohrbach, S. Venugopalan, K. Saenko, and T. Darrell. Long-term recurrent convolutional networks for visual recognition and description. *CoRR*, abs/1411.4389, 2014.

[11] A. Dosovitskiy, L. Beyer, A. Kolesnikov, D. Weissenborn, X. Zhai, T. Unterthiner, M. Dehghani, M. Minderer, G. Heigold, S. Gelly, J. Uszkoreit, and N. Houlsby. An image is worth 16x16 words: Transformers for image recognition at scale. *CoRR*, abs/2010.11929, 2020.

[12] C. Feichtenhofer. X3D: expanding architectures for efficient video recognition. *CoRR*, abs/2004.04730, 2020.

[13] C. Feichtenhofer, H. Fan, J. Malik, and K. He. Slowfast networks for video recognition. *CoRR*, abs/1812.03982, 2018.

[14] K. He, X. Zhang, S. Ren, and J. Sun. Deep residual learning for image recognition. *CoRR*, abs/1512.03385, 2015.

[15] S. He and S.-H. G. Chan. Wi-fi fingerprint-based indoor positioning: Recent advances and comparisons. *IEEE Communications Surveys and Tutorials*, 18(1):466–490, 2016.

[16] A. Howard, M. Sandler, G. Chu, L. Chen, B. Chen, M. Tan, W. Wang, Y. Zhu, R. Pang, V. Vasudevan, Q. V. Le, and H. Adam. Searching for mobilenetv3. *CoRR*, abs/1905.02244, 2019.

[17] G. Huang, Z. Liu, and K. Q. Weinberger. Densely connected convolutional networks. *CoRR*, abs/1608.06993, 2016.

[18] W. Kay, J. Carreira, K. Simonyan, B. Zhang, C. Hillier, S. Vijayanarasimhan, F. Viola, T. Green, T. Back, P. Natsev, M. Suleyman, and A. Zisserman. The kinetics human action video dataset. *CoRR*, abs/1705.06950, 2017.

[19] A. Khalajmehrabadi, N. Gatsis, and D. Akopian. Modern WLAN fingerprinting indoor positioning methods and deployment challenges. *CoRR*, abs/1610.05424, 2016.

[20] G. Klein and D. Murray. Parallel tracking and mapping for small ar workspaces. In *2007 6th IEEE and ACM International Symposium on Mixed and Augmented Reality*, pages 225–234, 2007.

[21] A. Krizhevsky, I. Sutskever, and G. E. Hinton. Imagenet classification with deep convolutional neural networks. In F. Pereira, C. J. C. Burges, L. Bottou, and K. Q. Weinberger, editors, *Advances in Neural Information Processing Systems 25*, pages 1097–1105. Curran Associates, Inc., 2012.

[22] Y. LeCun, L. Bottou, Y. Bengio, and P. Haffner. Gradient-based learning applied to document recognition. In *Proceedings of the IEEE*, volume 86, pages 2278–2324, 1998.

[23] Z. Liu, H. Mao, C. Wu, C. Feichtenhofer, T. Darrell, and S. Xie. A convnet for the 2020s. *CoRR*, abs/2201.03545, 2022.

[24] I. Loshchilov and F. Hutter. Fixing weight decay regularization in adam. *CoRR*, abs/1711.05101, 2017.

[25] R. Mur-Artal, J. M. M. Montiel, and J. D. Tardós. ORB-SLAM: a versatile and accurate monocular SLAM system. *CoRR*, abs/1502.00956, 2015.

[26] K. Simonyan and A. Zisserman. Very deep convolutional networks for large-scale image recognition. *CoRR*, abs/1409.1556, 2014.

[27] C. Szegedy, W. Liu, Y. Jia, P. Sermanet, S. E. Reed, D. Anguelov, D. Erhan, V. Vanhoucke, and A. Rabinovich. Going deeper with convolutions. *CoRR*, abs/1409.4842, 2014.

[28] A. Tahat, G. Kaddoum, S. Yousefi, S. Valaee, and F. Gagnon. A look at the recent wireless positioning techniques with a focus on algorithms for moving receivers. *IEEE Access*, 4:6652 – 6680, 09 2016.

[29] M. Tan and Q. V. Le. Efficientnetv2: Smaller models and faster training. *CoRR*, abs/2104.00298, 2021.

[30] D. Tran, L. D. Bourdev, R. Fergus, L. Torresani, and M. Paluri. C3D: generic features for video analysis. *CoRR*, abs/1412.0767, 2014.

[31] D. Tran, H. Wang, L. Torresani, J. Ray, Y. LeCun, and M. Paluri. A closer look at spatiotemporal convolutions for action recognition. *CoRR*, abs/1711.11248, 2017.

[32] A. Vaswani, N. Shazeer, N. Parmar, J. Uszkoreit, L. Jones, A. N. Gomez, L. Kaiser, and I. Polosukhin. Attention is all you need. *CoRR*, abs/1706.03762, 2017.

[33] S. Wang, R. Clark, H. Wen, and N. Trigoni. Deepvo: Towards end-to-end visual odometry with deep recurrent convolutional neural networks. *CoRR*, abs/1709.08429, 2017.

7 Appendix

7.1 Reproducibility

All code and data used in this project is available on GitHub. The project's `README` file contains detailed instructions on how to reproduce the results of this project.

Further, the precise configuration and results of the experiments that are reported here are publicly available as a public Weights & Biases experiments.

7.2 Machine Specifications

Table 4 lists the two machines, alongside relevant specifications, that were used for training and evaluation of the models. The HPC cluster was used for training and evaluation of all models. Analyses and visualisations were performed on the local machine, as well as running the real-time inference demo.

	Specification	Value
Sys.	Name	Darwin
	Node	MacBook Pro
CPU	Model	Apple M1
	Architecture	ARM64
	Physical Cores	8
	Frequency	2.4 GHz
Mem.	Total Capacity	16 GB
	Avg. Used Capacity	~ 7.4 GB

(a) Local Machine

	Specification	Value
Sys.	Name	Linux
	Node	Desktop 24
CPU	Model	Intel(R) Xeon(R) CPU E5-2660 v3 @ 2.60GHz
	Architecture	x86_64
	Physical Cores	20
	Frequency	3.3 GHz
GPU	Model	NVIDIA GeForce GTX 1080 Ti
	Memory	11.2 GB
Mem.	Total Capacity	250 GB
	Avg. Used Capacity	~ 7.4 GB

(b) HPC (Remote Server)

Table 4: **Machine Specifications.** The Table shows relevant hardware specifications for (a) the local machine and (b) the remote server that were used for conducting experiments within this study.